Study of $J/\psi \to p\bar{p}$ and $J/\psi \to n\bar{n}$

M. Ablikim,[1] M. N. Achasov,[5] D. J. Ambrose,[40] F. F. An,[1] Q. An,[41] Z. H. An,[1] J. Z. Bai,[1] Y. Ban,[27] J. Becker,[2] N. Berger,[1] M. Bertani,[18] J. M. Bian,[39] E. Boger,[20,*] O. Bondarenko,[21] I. Boyko,[20] R. A. Briere,[3] V. Bytev,[20] X. Cai,[1] A. Calcaterra,[18] G. F. Cao,[1] J. F. Chang,[1] G. Chelkov,[20,*] G. Chen,[1] H. S. Chen,[1] J. C. Chen,[1] M. L. Chen,[1] S. J. Chen,[25] Y. Chen,[1] Y. B. Chen,[1] H. P. Cheng,[14] Y. P. Chu,[1] D. Cronin-Hennessy,[39] H. L. Dai,[1] J. P. Dai,[1] D. Dedovich,[20] Z. Y. Deng,[1] A. Denig,[19] I. Denysenko,[20,†] M. Destefanis,[44] W. M. Ding,[29] Y. Ding,[23] L. Y. Dong,[1] M. Y. Dong,[1] S. X. Du,[47] J. Fang,[1] S. S. Fang,[1] L. Fava,[44,‡] F. Feldbauer,[2] C. Q. Feng,[41] R. B. Ferroli,[18] C. D. Fu,[1] J. L. Fu,[25] Y. Gao,[36] C. Geng,[41] K. Goetzen,[7] W. X. Gong,[1] W. Gradl,[19] M. Greco,[44] M. H. Gu,[1] Y. T. Gu,[9] Y. H. Guan,[6] A. Q. Guo,[26] L. B. Guo,[24] Y. P. Guo,[26] Y. L. Han,[1] X. Q. Hao,[1] F. A. Harris,[38] K. L. He,[1] M. He,[1] Z. Y. He,[26] T. Held,[2] Y. K. Heng,[1] Z. L. Hou,[1] H. M. Hu,[1] J. F. Hu,[6] T. Hu,[1] B. Huang,[1] G. M. Huang,[15] J. S. Huang,[12] X. T. Huang,[29] Y. P. Huang,[1] T. Hussain,[43] C. S. Ji,[41] Q. Ji,[1] X. B. Ji,[1] X. L. Ji,[1] L. K. Jia,[1] L. L. Jiang,[1] X. S. Jiang,[1] J. B. Jiao,[29] Z. Jiao,[14] D. P. Jin,[1] S. Jin,[1] F. F. Jing,[36] N. Kalantar-Nayestanaki,[21] M. Kavatsyuk,[21] W. Kuehn,[37] W. Lai,[1] J. S. Lange,[37] J. K. C. Leung,[35] C. H. Li,[1] Cheng Li,[41] Cui Li,[41] D. M. Li,[47] F. Li,[1] G. Li,[1] H. B. Li,[1] J. C. Li,[1] K. Li,[10] Lei Li,[1] N. B. Li,[24] Q. J. Li,[1] S. L. Li,[1] W. D. Li,[1] W. G. Li,[1] X. L. Li,[29] X. N. Li,[1] X. Q. Li,[26] X. R. Li,[28] Z. B. Li,[33] H. Liang,[41] Y. F. Liang,[31] Y. T. Liang,[37] G. R. Liao,[36] X. T. Liao,[1] B. J. Liu,[34] B. J. Liu,[1] C. L. Liu,[3] C. X. Liu,[1] C. Y. Liu,[1] F. H. Liu,[30] Fang Liu,[1] Feng Liu,[15] H. Liu,[1] H. B. Liu,[6] H. H. Liu,[13] H. M. Liu,[1] H. W. Liu,[1] J. P. Liu,[45] K. Y. Liu,[23] Kai Liu,[6] Kun Liu,[27] P. L. Liu,[29] S. B. Liu,[41] X. Liu,[22] X. H. Liu,[1] Y. Liu,[1] Y. B. Liu,[26] Z. A. Liu,[1] Zhiqiang Liu,[1] Zhiqing Liu,[1] H. Loehner,[21] G. R. Lu,[12] H. J. Lu,[14] J. G. Lu,[1] Q. W. Lu,[30] X. R. Lu,[6] Y. P. Lu,[1] C. L. Luo,[24] M. X. Luo,[46] T. Luo,[38] X. L. Luo,[1] M. Lv,[1] C. L. Ma,[6] F. C. Ma,[23] H. L. Ma,[1] Q. M. Ma,[1] S. Ma,[1] T. Ma,[1] X. Y. Ma,[1] Y. Ma,[11] F. E. Maas,[11] M. Maggiora,[44] Q. A. Malik,[43] H. Mao,[1] Y. J. Mao,[27] Z. P. Mao,[1] J. G. Messchendorp,[21] J. Min,[1] T. J. Min,[1] R. E. Mitchell,[17] X. H. Mo,[1] C. Morales Morales,[11] C. Motzko,[2] N. Yu. Muchnoi,[5] Y. Nefedov,[20] C. Nicholson,[6] I. B. Nikolaev,[5] Z. Ning,[1] S. L. Olsen,[28] Q. Ouyang,[1] S. Pacetti,[18,§] J. W. Park,[28] M. Pelizaeus,[38] K. Peters,[7] J. L. Ping,[24] R. G. Ping,[1] R. Poling,[39] E. Prencipe,[19] C. S. J. Pun,[35] M. Qi,[25] S. Qian,[1] C. F. Qiao,[6] X. S. Qin,[1] Y. Qin,[27] Z. H. Qin,[1] J. F. Qiu,[1] K. H. Rashid,[43] G. Rong,[1] X. D. Ruan,[9] A. Sarantsev,[20,‖] J. Schulze,[2] M. Shao,[41] C. P. Shen,[38,¶] X. Y. Shen,[1] H. Y. Sheng,[1] M. R. Shepherd,[17] X. Y. Song,[1] S. Spataro,[44] B. Spruck,[37] D. H. Sun,[1] G. X. Sun,[1] J. F. Sun,[12] S. S. Sun,[1] X. D. Sun,[1] Y. J. Sun,[41] Y. Z. Sun,[1] Z. J. Sun,[1] Z. T. Sun,[41] C. J. Tang,[31] X. Tang,[1] E. H. Thorndike,[40] H. L. Tian,[1] D. Toth,[39] M. Ullrich,[37] G. S. Varner,[38] B. Wang,[9] B. Q. Wang,[27] K. Wang,[1] L. L. Wang,[4] L. S. Wang,[1] M. Wang,[29] P. Wang,[1] P. L. Wang,[1] Q. Wang,[1] Q. J. Wang,[1] S. G. Wang,[27] X. F. Wang,[12] X. L. Wang,[41] Y. D. Wang,[41] Y. F. Wang,[1] Y. Q. Wang,[29] Z. Wang,[1] Z. G. Wang,[1] Z. Y. Wang,[1] D. H. Wei,[8] P. Weidenkaff,[19] Q. G. Wen,[41] S. P. Wen,[1] M. Werner,[37] U. Wiedner,[2] L. H. Wu,[1] N. Wu,[1] S. X. Wu,[41] W. Wu,[26] Z. Wu,[1] L. G. Xia,[36] Z. J. Xiao,[24] Y. G. Xie,[1] Q. L. Xiu,[1] G. F. Xu,[1] G. M. Xu,[27] H. Xu,[1] Q. J. Xu,[10] X. P. Xu,[32] Y. Xu,[26] Z. R. Xu,[41] F. Xue,[15] Z. Xue,[1] L. Yan,[41] W. B. Yan,[41] Y. H. Yan,[16] H. X. Yang,[1] T. Yang,[9] Y. Yang,[15] Y. X. Yang,[8] H. Ye,[1] M. Ye,[1] M. H. Ye,[4] B. X. Yu,[1] C. X. Yu,[26] J. S. Yu,[22] S. P. Yu,[29] C. Z. Yuan,[1] W. L. Yuan,[24] Y. Yuan,[1] A. A. Zafar,[43] A. Zallo,[18] Y. Zeng,[16] B. X. Zhang,[1] B. Y. Zhang,[1] C. C. Zhang,[1] D. H. Zhang,[1] H. H. Zhang,[33] H. Y. Zhang,[1] J. Zhang,[24] J. G. Zhang,[12] J. Q. Zhang,[1] J. W. Zhang,[1] J. Y. Zhang,[1] J. Z. Zhang,[1] L. Zhang,[25] S. H. Zhang,[1] T. R. Zhang,[24] X. J. Zhang,[1] X. Y. Zhang,[29] Y. Zhang,[1] Y. H. Zhang,[1] Y. S. Zhang,[9] Z. P. Zhang,[41] Z. Y. Zhang,[45] G. Zhao,[1] H. S. Zhao,[1] J. W. Zhao,[1] K. X. Zhao,[24] Lei Zhao,[41] Ling Zhao,[1] M. G. Zhao,[26] Q. Zhao,[1] S. J. Zhao,[47] T. C. Zhao,[1] X. H. Zhao,[25] Y. B. Zhao,[1] Z. G. Zhao,[41] A. Zhemchugov,[20,*] B. Zheng,[42] J. P. Zheng,[1] Y. H. Zheng,[6] Z. P. Zheng,[1] B. Zhong,[1] J. Zhong,[2] L. Zhou,[1] X. K. Zhou,[6] X. R. Zhou,[41] C. Zhu,[1] K. Zhu,[1] K. J. Zhu,[1] S. H. Zhu,[1] X. L. Zhu,[36] X. W. Zhu,[1] Y. M. Zhu,[26] Y. S. Zhu,[1] Z. A. Zhu,[1] J. Zhuang,[1] B. S. Zou,[1] J. H. Zou,[1] and J. X. Zuo[1]

(BESIII Collaboration)

[1]*Institute of High Energy Physics, Beijing 100049, People's Republic of China*
[2]*Bochum Ruhr-University, 44780 Bochum, Germany*
[3]*Carnegie Mellon University, Pittsburgh, Pennsylvania 15213, USA*
[4]*China Center of Advanced Science and Technology, Beijing 100190, People's Republic of China*
[5]*G. I. Budker Institute of Nuclear Physics SB RAS (BINP), Novosibirsk 630090, Russia*
[6]*Graduate University of Chinese Academy of Sciences, Beijing 100049, People's Republic of China*
[7]*GSI Helmholtzcentre for Heavy Ion Research GmbH, D-64291 Darmstadt, Germany*
[8]*Guangxi Normal University, Guilin 541004, People's Republic of China*
[9]*GuangXi University, Nanning 530004, People's Republic of China*
[10]*Hangzhou Normal University, Hangzhou 310036, People's Republic of China*
[11]*Helmholtz Institute Mainz, J. J. Becherweg 45,D 55099 Mainz, Germany*

[12]*Henan Normal University, Xinxiang 453007, People's Republic of China*
[13]*Henan University of Science and Technology, Luoyang 471003, People's Republic of China*
[14]*Huangshan College, Huangshan 245000, People's Republic of China*
[15]*Huazhong Normal University, Wuhan 430079, People's Republic of China*
[16]*Hunan University, Changsha 410082, People's Republic of China*
[17]*Indiana University, Bloomington, Indiana 47405, USA*
[18]*INFN Laboratori Nazionali di Frascati, Frascati, Italy*
[19]*Johannes Gutenberg University of Mainz, Johann-Joachim-Becher-Weg 45, 55099 Mainz, Germany*
[20]*Joint Institute for Nuclear Research, 141980 Dubna, Russia*
[21]*KVI/University of Groningen, 9747 AA Groningen, The Netherlands*
[22]*Lanzhou University, Lanzhou 730000, People's Republic of China*
[23]*Liaoning University, Shenyang 110036, People's Republic of China*
[24]*Nanjing Normal University, Nanjing 210046, People's Republic of China*
[25]*Nanjing University, Nanjing 210093, People's Republic of China*
[26]*Nankai University, Tianjin 300071, People's Republic of China*
[27]*Peking University, Beijing 100871, People's Republic of China*
[28]*Seoul National University, Seoul, 151-747 Korea*
[29]*Shandong University, Jinan 250100, People's Republic of China*
[30]*Shanxi University, Taiyuan 030006, People's Republic of China*
[31]*Sichuan University, Chengdu 610064, People's Republic of China*
[32]*Soochow University, Suzhou 215006, People's Republic of China*
[33]*Sun Yat-Sen University, Guangzhou 510275, People's Republic of China*
[34]*The Chinese University of Hong Kong, Shatin, N. T., Hong Kong*
[35]*The University of Hong Kong, Pokfulam, Hong Kong*
[36]*Tsinghua University, Beijing 100084, People's Republic of China*
[37]*Universitaet Giessen, 35392 Giessen, Germany*
[38]*University of Hawaii, Honolulu, Hawaii 96822, USA*
[39]*University of Minnesota, Minneapolis, Minnesota 55455, USA*
[40]*University of Rochester, Rochester, New York 14627, USA*
[41]*University of Science and Technology of China, Hefei 230026, People's Republic of China*
[42]*University of South China, Hengyang 421001, People's Republic of China*
[43]*University of the Punjab, Lahore-54590, Pakistan*
[44]*University of Turin and INFN, Turin, Italy*
[45]*Wuhan University, Wuhan 430072, People's Republic of China*
[46]*Zhejiang University, Hangzhou 310027, People's Republic of China*
[47]*Zhengzhou University, Zhengzhou 450001, People's Republic of China*

(Received 4 May 2012; published 31 August 2012)

The decays $J/\psi \to p\bar{p}$ and $J/\psi \to n\bar{n}$ have been investigated with a sample of 225.2×10^6 J/ψ events collected with the BESIII detector at the BEPCII e^+e^- collider. The branching fractions are determined to be $\mathcal{B}(J/\psi \to p\bar{p}) = (2.112 \pm 0.004 \pm 0.031) \times 10^{-3}$ and $\mathcal{B}(J/\psi \to n\bar{n}) = (2.07 \pm 0.01 \pm 0.17) \times 10^{-3}$. Distributions of the angle θ between the proton or antineutron and the beam direction are well described by the form $1 + \alpha\cos^2\theta$, and we find $\alpha = 0.595 \pm 0.012 \pm 0.015$ for $J/\psi \to p\bar{p}$ and $\alpha = 0.50 \pm 0.04 \pm 0.21$ for $J/\psi \to n\bar{n}$. Our branching-fraction results suggest a large phase angle between the strong and electromagnetic amplitudes describing the $J/\psi \to N\bar{N}$ decay.

DOI: 10.1103/PhysRevD.86.032014 PACS numbers: 14.40.Pq, 12.38.Qk, 13.25.Gv

I. INTRODUCTION

The J/ψ meson is interpreted as a bound state of a charmed quark and a charmed antiquark ($c\bar{c}$). The decay process $J/\psi \to N\bar{N}$ ($N = p$ or n) is an octet-baryon-pair decay mode, and should be a good laboratory for testing perturbative QCD (pQCD) because the three gluons in the OZI-violating strong decay correspond to the three $q\bar{q}$ pairs that form the final-state nucleons. The ratio of the branching fractions for the $p\bar{p}$ and $n\bar{n}$ final states provides information about the phase angle between the strong and the electromagnetic (EM) amplitudes governing the decay

*Also at the Moscow Institute of Physics and Technology, Moscow, Russia
†On leave from the Bogolyubov Institute for Theoretical Physics, Kiev, Ukraine
‡University of Piemonte Orientale and INFN (Turin)
§University and INFN of Perugia, Perugia, Italy
‖Also at the PNPI, Gatchina, Russia
¶Now at Nagoya University, Nagoya, Japan

[1–3]. Because the initial-state isospin is 0, the strong-decay amplitudes for the $p\bar{p}$ and $n\bar{n}$ final states must be equal. The $J/\psi \to p\bar{p}$ and $J/\psi \to n\bar{n}$ EM decays are expected to have amplitudes that are of about the same magnitude, but with opposite signs, like the magnetic moments (as discussed in Sec. VII). Because the EM decays of J/ψ to $p\bar{p}$ and $n\bar{n}$ behave the same as nonresonant production of those final states, the magnitude of the EM decay amplitude of J/ψ can be estimated from the cross section for continuum production $e^+e^- \to p\bar{p}$. If the strong and EM amplitudes are almost real, and therefore in phase, as predicted by pQCD [1–5], then interference would lead to a branching fraction for $J/\psi \to n\bar{n}$ about one-half as large as that for $J/\psi \to p\bar{p}$. Conversely, if the strong and EM amplitudes are orthogonal, then the strong decay dominates and the branching fractions are expected to be equal. In previous experiments, $J/\psi \to p\bar{p}$ has been measured with good precision, while $J/\psi \to n\bar{n}$ has been measured with quite a large uncertainty [6,7]. They appear to be equal within errors, at odds with the pQCD expectation.

The angular distribution for $J/\psi \to N\bar{N}$ can be written as a function of the angle θ between the nucleon or antinucleon direction and the beam as follows:

$$\frac{dN}{d\cos\theta} = A(1 + \alpha\cos^2\theta),$$

where A is an overall normalization. These angular distributions reflect details of the baryon structure and have the potential to distinguish among different theoretical models [1–5].

In this paper, we report new studies of the process $J/\psi \to N\bar{N}$ made with the BESIII detector at the BEPCII electron-positron storage ring [8,9]. With the world's largest sample of J/ψ decays, we obtain improved measurements for the $J/\psi \to p\bar{p}$ and $J/\psi \to n\bar{n}$ branching fractions and angular distributions.

II. BEPCII AND BESIII

BEPCII is a two-ring e^+e^- collider designed for a peak luminosity of 10^{33} cm$^{-2}s^{-1}$ at a beam current of 0.93 A. The cylindrical core of the BESIII detector consists of a helium-gas-based drift chamber (MDC) for charged-particle tracking and particle identification by dE/dx, a plastic scintillator time-of-flight system (TOF) for additional particle identification, and a 6240-crystal CsI(Tl) Electromagnetic Calorimeter (EMC) for electron identification and photon detection. These components are all enclosed in a superconducting solenoidal magnet providing a 1.0-T magnetic field. The solenoid is supported by an octagonal flux-return yoke with resistive-plate-counter muon detector modules (MU) interleaved with steel. The geometrical acceptance for charged tracks and photons is 93% of 4π, and the resolutions for charged-track momentum and photon energy at 1 GeV are 0.5% and 2.5%, respectively. More details on the features and capabilities of BESIII are provided in Ref. [8].

III. DATA SAMPLE

Our data sample consists of 225.2×10^6 $e^+e^- \to J/\psi$ events collected during 2009. The estimated uncertainty in the number of events is $\pm 1.3\%$ [10]. A GEANT4-based [11,12] detector simulation is used to produce Monte Carlo (MC) samples for signal and background processes that are generated with specialized models that have been packaged and customized for BESIII [13]. EVTGEN [14] is used to study phase-space signal events for $J/\psi \to p\bar{p}$ and for exclusive backgrounds in J/ψ decays. BABAYAGA [15] is used to generate Bhabha and $\gamma\gamma$ events as possible EM backgrounds. A large inclusive sample (200×10^6 events) is used to simulate hadronic background processes. The J/ψ resonance is generated by KKMC [16]. Known J/ψ decay modes are generated with EVTGEN, using branching fractions set to world-average values [6]. The remaining J/ψ decay modes are generated by LUNDCHARM [13], which is based on JETSET [17] and tuned for the charm-energy region. The decays $J/\psi \to p\bar{p}$ and $J/\psi \to n\bar{n}$ are excluded from this sample.

IV. GENERAL EVENT SELECTION

Charged tracks in BESIII are reconstructed from MDC hits. To optimize the momentum measurement, we select tracks in the polar angle range $|\cos\theta| < 0.93$ and require that they pass within ± 10 cm of the interaction point in the beam direction and within ± 1 cm in the plane perpendicular to the beam.

Electromagnetic showers are reconstructed by clustering EMC crystal energies. Efficiency and energy resolution are improved by including energy deposits in nearby TOF counters. Showers used in selecting photons and in π^0 reconstruction must satisfy fiducial and shower-quality requirements. Showers in the barrel region ($|\cos\theta| < 0.8$) must have a minimum energy of 25 MeV, while those in the endcaps ($0.86 < |\cos\theta| < 0.92$) must have at least 50 MeV. Showers in the region between the barrel and endcap are poorly reconstructed and are excluded. To eliminate showers from charged particles, a photon must be separated by at least 10° from any charged track. EMC timing requirements suppress electronic noise and energy deposits unrelated to the event.

V. ANALYSIS OF $J/\psi \to p\bar{p}$

A. Event selection

Events with exactly two good charged tracks in the polar angle range $|\cos\theta| < 0.8$ are selected. We exclude the two endcap regions to reduce systematic uncertainties in tracking and particle identification. By using a loose particle-identification requirement for the positive track (probability of the p hypothesis greater than the probabilities for the π^+

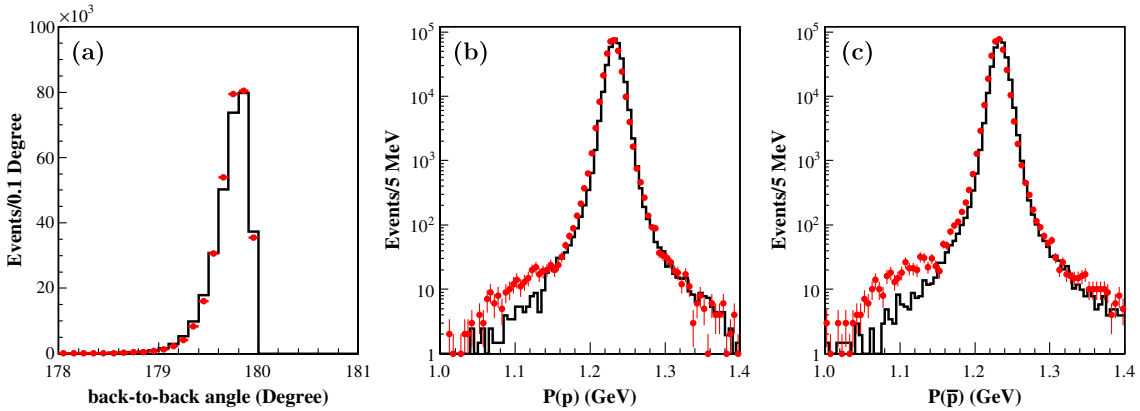

FIG. 1 (color online). Comparisons between data (points) and MC (histograms) for properties of the p and $\bar{p}$ tracks for selected $J/\psi \to p\bar{p}$ signal events: (a) angle between the p and $\bar{p}$, (b) p momentum, and (c) $\bar{p}$ momentum.

and K^+ hypotheses), and by requiring no particle identification for the negative track, the efficiency is maximized and the systematic uncertainty is minimized. A vertex fit is performed to the two selected tracks to improve the momentum resolution, and the angle between the p and $\bar{p}$ is required to be greater than 178°. Finally, for both tracks, the measured momentum magnitude must be within 30 MeV/c ($\sim 3\sigma$) of the expected value of 1.232 GeV/c. Figure 1 shows comparisons between data and MC for the angle between the p and $\bar{p}$ and for their momenta.

This selection results in a signal of $N = 314651 \pm 561$ candidate events. Figures 1(b) and 1(c) show the p and $\bar{p}$ momentum distributions for these events, along with the expected distributions for a pure MC $J/\psi \to p\bar{p}$ signal. Backgrounds overall are very small, and appear to be negligible in the accepted p and $\bar{p}$ momentum range. Three independent procedures are used to estimate this background: inclusive J/ψ MC, exclusive MC of potential background processes (Bhabha events and J/ψ decays to e^+e^-, $\mu^+\mu^-$, K^+K^-, $\gamma p\bar{p}$, $\pi^0 p\bar{p}$, and $\gamma\eta_c$ with $\eta_c \to p\bar{p}$), and a sideband technique. The estimates range from 0.02% to 0.2% of the signal. We apply no subtraction and take the largest of the estimates (sideband) as a systematic uncertainty in the final result. The raw distribution of $\cos\theta$ for the protons in the selected signal events is given in Fig. 2.

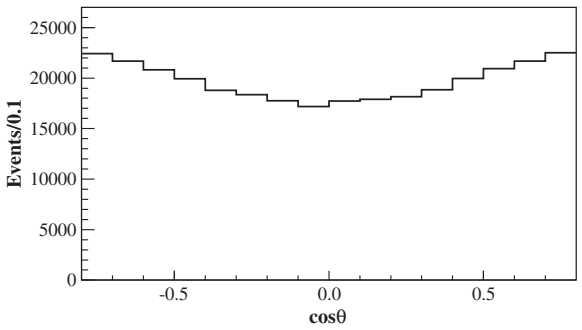

FIG. 2. Angular distribution of the selected $J/\psi \to p\bar{p}$ candidates.

B. Efficiency correction

To measure the $J/\psi \to p\bar{p}$ branching fraction and angular distribution, it is necessary to correct for the selection efficiency, which is dominated by track reconstruction and selection and by particle-identification efficiency. We use signal MC to obtain the efficiency, but use data to correct for imperfections in the simulation, thereby reducing the systematic uncertainty in the correction. We measure differences between the data and MC separately for the efficiencies of tracking and particle identification, leaving the other selection cuts in place or tightening them for cleaner selection. The correlation between the corrections in the tracking and particle-identification efficiencies has been shown in MC studies to be small, so we combine them into a single correction function that is applied to the MC-determined efficiency. Because the tracking and TOF response depend on the track direction, the efficiency correction is determined in bins of $\cos\theta$.

We divide the full angular range ($|\cos\theta| < 0.8$) into 16 equal bins and for each bin compute the efficiency for the successful reconstruction of the $\bar{p}$ or p track as follows:

$$\epsilon_{\rm trk} = \frac{N_2}{N_1 + N_2},$$

where N_1 (N_2) is the number of $J/\psi \to p\bar{p}$ events with 1 (2) good charged track(s) detected. For N_1, we require only one good charged track which is identified as a p or $\bar{p}$. Note that in this case, unlike the $J/\psi \to p\bar{p}$ selection, we can apply particle identification to the $\bar{p}$ selection to improve purity, since any inconsistency between data and MC would cancel in the efficiency. Figure 3 shows the data/MC comparison for the tracking efficiencies and the computed correction factor $\epsilon_{\rm trk}^{\rm data}/\epsilon_{\rm trk}^{\rm MC}$ for each $\cos\theta$ bin for p and $\bar{p}$.

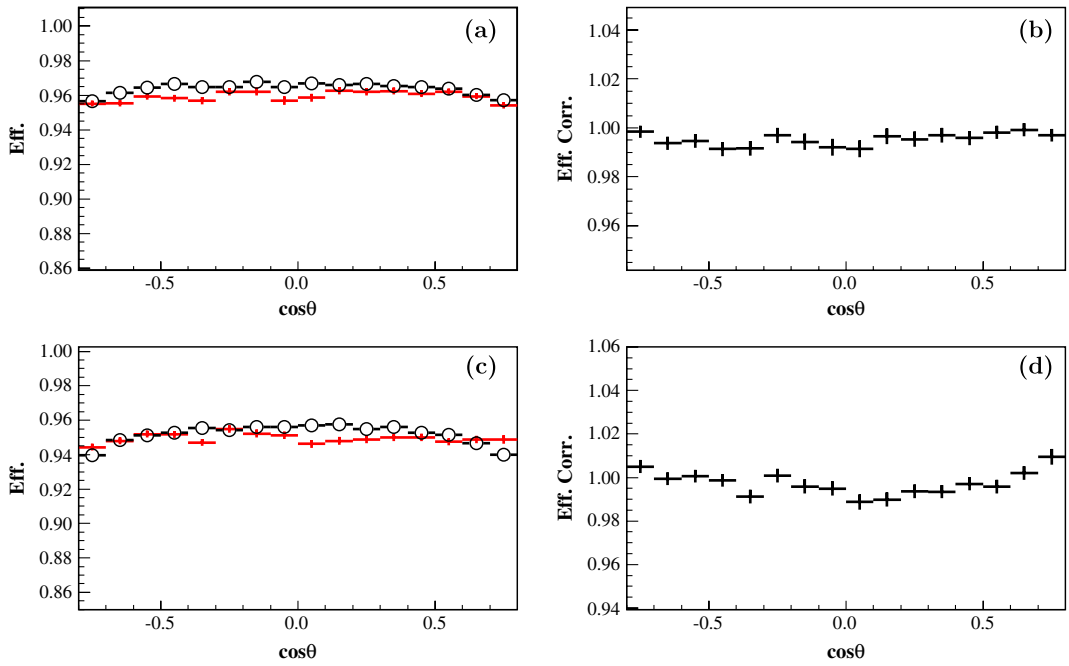

FIG. 3 (color online). (a) The proton tracking efficiency for data (points) and MC (circles), and (b) the correction $\epsilon_{\rm trk}^{\rm data}/\epsilon_{\rm trk}^{\rm MC}$; (c) and (d) show the same for antiprotons.

We can similarly measure the particle-identification efficiency for the p in each $\cos\theta$ bin, considering only $J/\psi \to p\bar{p}$ events in which there are two good charged tracks, with the negatively-charged track identified as an antiproton. We define the efficiency as follows:

$$\epsilon_{\rm pid} = \frac{N_p}{N_p + N_{\not p}},$$

where N_p is the number of selected events in which the proton has been successfully identified and $N_{\not p}$ is the number of events without the proton identified. To select a more pure sample we tighten the selection on the p and $\bar{p}$ momenta to be within 20 MeV/c ($\sim 2\sigma$) of the expected value. Figure 4 shows the data/MC comparison for the proton particle identification efficiency and the resulting correction factor $\epsilon_{\rm pid}^{\rm data}/\epsilon_{\rm pid}^{\rm MC}$.

In each $\cos\theta$ bin, the corrected MC-determined efficiency to be applied to data is computed with the following formula:

$$\epsilon = \epsilon^{\rm MC} \times \frac{\epsilon_{p\rm trk}^{\rm data}}{\epsilon_{p\rm trk}^{\rm MC}} \times \frac{\epsilon_{p\rm pid}^{\rm data}}{\epsilon_{p\rm pid}^{\rm MC}} \times \frac{\epsilon_{\bar{p}\rm trk}^{\rm data}}{\epsilon_{\bar{p}\rm trk}^{\rm MC}}.$$

To diminish the effect of bin-to-bin scatter due to statistical fluctuations, we fit the corrected efficiency as a function of $\cos\theta$ with a fifth-order polynomial, as shown in Fig. 5.

C. Angular distribution and branching fraction

We fit the measured angular distribution of the proton from $J/\psi \to p\bar{p}$ to the function $A(1 + \alpha\cos^2\theta)\epsilon(\cos\theta)$, where A is the overall normalization and $\epsilon(\cos\theta)$ is the

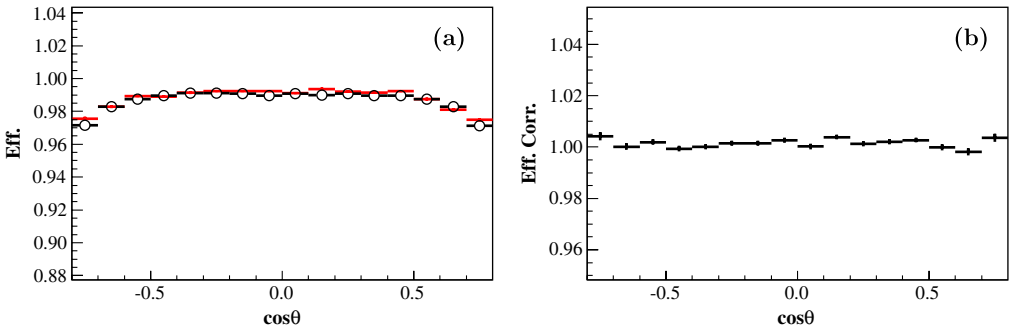

FIG. 4 (color online). (a) p particle-identification efficiency for data (points) and MC (circles), and (b) the computed efficiency correction factor $\epsilon_{\rm pid}^{\rm data}/\epsilon_{\rm pid}^{\rm MC}$.

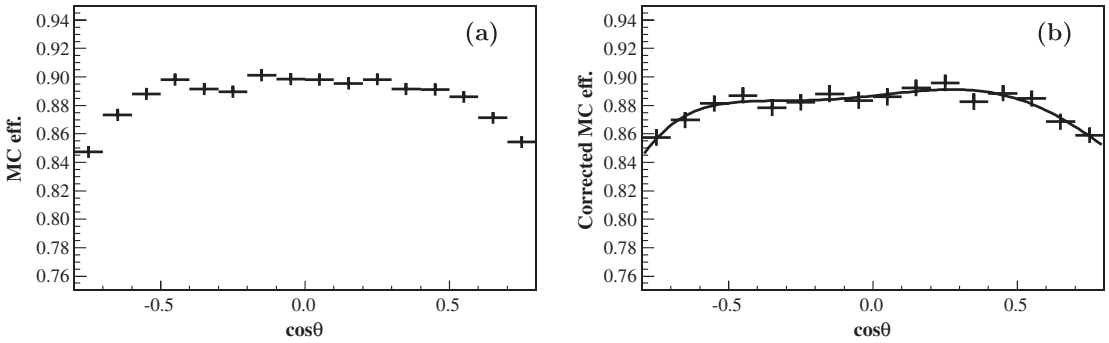

FIG. 5. $J/\psi \to p\bar{p}$ selection efficiency as a function of $\cos\theta$ (a) before correction, and (b) after correction. The line shows the smoothed efficiency obtained by fitting the data to a fifth-order polynomial.

corrected MC-determined efficiency function (Sec. V B). The angular distribution and the fit are shown in Fig. 6. The χ^2 for the fit is 16, with 14 degrees of freedom, and the value determined for the angular-distribution parameter is $\alpha = 0.595 \pm 0.012$, where the error is statistical only.

The raw yield of $J/\psi \to p\bar{p}$ events obtained by counting protons in the angular range $\cos\theta = [-0.8, 0.8]$ is $N(-0.8, 0.8) = 314651 \pm 561$. The efficiency-corrected yield obtained by fitting the $\cos\theta$ distribution over this range is $N_{\rm cor}(-0.8, 0.8) = 357786 \pm 638$. The fitted value of α is used to determine the total number of $J/\psi \to n\bar{n}$ events in the full angular range of $\cos\theta = [-1.0, 1.0]$ as follows:

$$N_{\rm cor}(-1.0, 1.0) = N_{\rm cor}(-0.8, 0.8) \times \frac{\int_{-1.0}^{1.0}(1 + \alpha\cos^2\theta)d\theta}{\int_{-0.8}^{0.8}(1 + \alpha\cos^2\theta)d\theta} = 475567 \pm 848.$$

Combining this final yield with the number of J/ψ events in our sample ($(2.252 \pm 0.029) \times 10^8$), we find the branching fraction to be

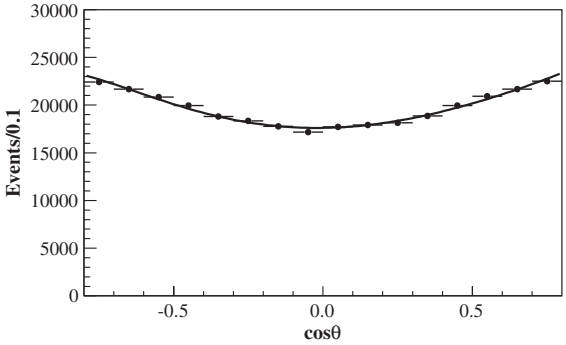

FIG. 6. The points represent the measured distribution of $\cos\theta$ for the p in $J/\psi \to p\bar{p}$ candidate events, with error bars that are the quadratic sums of the statistical and efficiency uncertainties. The line represents the fit of the distribution to the functional form given in the text, and is used to determine the normalization and the angular-distribution parameter α.

$$\mathcal{B}(J/\psi \to p\bar{p}) = (2.112 \pm 0.004) \times 10^{-3},$$

where the error is statistical only.

D. Systematic errors and results

To determine the uncertainty in the efficiency correction, we use toy MC experiments to obtain distributions in the branching fraction and α that reflect the statistical errors of the bin-by-bin efficiency values. We perform this study by varying each bin randomly according to a normal distribution for each MC experiment, redoing the polynomial fit and then remeasuring the efficiency-corrected yield. The results have normal distributions and they are fitted with Gaussian functions to estimate the associated uncertainties in the branching fraction and α, which are found to be 4.69×10^{-6} and 0.011, respectively.

The full magnitude of the $p\bar{p}$ momentum sideband background estimate (0.2%) is taken to be the uncertainty in the branching fraction due to the background correction. We fit the sideband-subtracted angular distribution and determine a new value for the angular parameter α, taking the change relative to the standard result (0.004) as the systematic error.

To estimate the systematic error due to the detector angular resolution, we perform a study with the signal MC. The ''true'' generated proton $\cos\theta$ is fitted before and after smearing with a MC-derived angular resolution function. The differences in the fitted α values (0.010) and in the branching fractions (4×10^{-6}) are taken as the systematic uncertainties from this source.

The branching fraction also incurs two systematic uncertainties that do not affect α. A small systematic uncertainty enters due to the correction for the $|\cos\theta| < 0.8$ requirement, which depends on the determined value of α and its error. The dominant uncertainty in the branching fraction is due to the estimated 1.3% error in the number of J/ψ events in our sample [10].

To study the effect from continuum production, we write the total cross section $\sigma_{p\bar{p}}$ as

TABLE I. Systematic errors for $J/\psi \to p\bar{p}$.

Sources	Effect on α	Effect on $\mathcal{B}(10^{-3})$
Efficiency Correction	0.011	0.005
Background	0.004	0.002
$\cos\theta$ Resolution	0.010	0.004
α Value	...	0.004
Number of J/ψ	...	0.026
continuum	...	0.015
Total	0.015	0.031

TABLE II. Previous measurements of α in $J/\psi \to p\bar{p}$.

Collaboration	α
Mark1 [18]	1.45 ± 0.56
Mark2 [19]	0.61 ± 0.23
Mark3 [20]	0.58 ± 0.14
DASP [21]	1.70 ± 1.70
DM2 [22]	0.62 ± 0.11
BESII [23]	0.676 ± 0.055

$$\sigma_{p\bar{p}} = |\sqrt{\sigma^{\text{cont.}}_{p\bar{p}}} + \frac{\sqrt{12\pi\Gamma_{ee}\Gamma_{\text{tot}}}}{s - m^2 + im\Gamma_{\text{tot}}}(E_p + e^{i\phi}S)|^2,$$

where E_p and S are the EM and strong amplitudes of $J/\psi \to p\bar{p}$ and ϕ is the phase angle between them. $\sigma^{\text{cont.}}_{p\bar{p}}$ is the $p\bar{p}$ cross section contributed by the continuum under the J/ψ peak. These values are taken from the calculation in Sec. VII. The difference with and without $\sigma^{\text{cont.}}_{p\bar{p}}$ is assigned as the systematic error.

Finally, we change α by $\pm 1\ \sigma$ (includes systematic error) and reevaluate the branching-fraction to estimate the systematic error in the branching-fraction measurement.

Table I provides a summary of all identified sources of systematic uncertainty, which are assumed to be uncorrelated, and their quadrature sum. The final results for our $J/\psi \to p\bar{p}$ measurements are as follows:

$$\alpha = 0.595 \pm 0.012 \pm 0.015, \quad \text{and}$$
$$\mathcal{B}(J/\psi \to p\bar{p}) = (2.112 \pm 0.004 \pm 0.031) \times 10^{-3}.$$

The branching-fraction measurement is consistent with the previous world average [6] and improves the overall precision by about a factor of 2.5. The value of α is also consistent with previous experiments (Table II) and is improved significantly.

VI. ANALYSIS OF $J/\psi \to n\bar{n}$

A. Event selection

We search for $J/\psi \to n\bar{n}$ candidates by selecting events that have no good charged tracks originating in the interaction region. The antineutron annihilation "star" in the EMC provides a signature for these events that is much more identifiable than the hadronic shower produced by a neutron. We therefore first select events with showers characteristic of $\bar{n}$ interactions, and then search in these events for energy deposited by n hadronic interactions on the opposite side of the detector.

The most energetic shower in the event is assigned to be the $\bar{n}$ candidate and is required to have an energy in the range 0.6–2.0 GeV. To optimize the discrimination against backgrounds, we apply a fiducial cut of $|\cos\theta| < 0.8$ to the $\bar{n}$ candidate. This ensures that the $\bar{n}$ energy is fully contained in the EMC for most signal events. To suppress photon backgrounds, we impose a requirement on the second moment of the candidate shower, defined as $S = \Sigma_i E_i r_i^2 / \Sigma_i E_i$, where E_i is the energy deposited in the ith crystal of the shower and r_i is the distance from the center of that crystal to the center of the shower. To be accepted, the $\bar{n}$ candidate must satisfy $S > 20$ cm^2. To further exploit the distinctive $\bar{n}$ shower topology, we require the number of EMC hits in a 50° cone around the $\bar{n}$ candidate shower direction to be greater than 40.

Events with accepted $\bar{n}$ candidates are searched for EMC showers on the opposite side of the detector that are consistent with being the neutron in a $J/\psi \to n\bar{n}$ decay. The energy of this shower must be between 0.06 and 0.6 GeV, a range found to be characteristic of the EMC neutron response in MC studies. If multiple showers are present, the one that is most back-to-back with respect to the $\bar{n}$ candidate is selected. To further suppress backgrounds from all-neutral J/ψ decays, continuum production and EM processes, we require $E_{\text{extra}} = 0$, where E_{extra} is the total deposited energy in the EMC, excluding that of the n shower and any additional energy in the 50° cone.

The expected signal for $J/\psi \to n\bar{n}$ is an enhancement near 180° in the distribution of the angle between the n shower and the direction of the $\bar{n}$. The distributions of this angle and of the cosine of the polar angle of the $\bar{n}$ shower ($\cos\theta$) for selected candidates are shown in Fig. 7. The enhancement near 180° in the distribution of the angle between the n and $\bar{n}$ constitutes the $J/\psi \to n\bar{n}$ signal. Since there is nonnegligible background, the number of $J/\psi \to n\bar{n}$ events must be determined by fitting. Distributions of the angle between the n and $\bar{n}$ are constructed in bins of $\cos\theta$ and fitted with signal and background functions.

Data-driven methods are used to determine the efficiency and signal shapes for $J/\psi \to n\bar{n}$. We select $J/\psi \to p(\bar{n})\pi^-$ and charge-conjugate (c.c.) events in data to obtain n and $\bar{n}$ samples to evaluate the selection efficiency. We use the p and $\bar{p}$ in $J/\psi \to p\bar{p}$ events that have been selected using information from just the MDC to get unbiased information on the shape and efficiency of the n and $\bar{n}$ response in the EMC, since antiproton and antineutron hadronic interactions are similar.

Generic J/ψ MC is used to assess the background. Figure 7(a) shows that there is no peaking in the

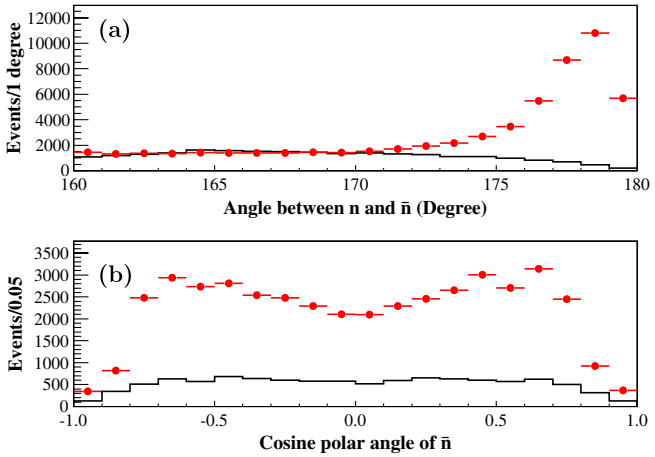

FIG. 7 (color online). Distributions for $J/\psi \to n\bar{n}$ candidate events summed over all $\cos\theta$ bins (points) and background from inclusive MC (solid lines): (a) angle between the n and $\bar{n}$, and (b) $\cos\theta$ for the $\bar{n}$ shower.

distribution of the angle between the n and $\bar{n}$ for this background. We also consider possible exclusive background channels: $J/\psi \to \pi^0 n\bar{n}$, $J/\psi \to \gamma n\bar{n}$, $e^+e^- \to \gamma\gamma$, $J/\psi \to \bar{\Sigma}^+\Sigma^-$, $J/\psi \to \Sigma^+\bar{\Sigma}^-$, $J/\psi \to p\bar{p}$, and $J/\psi \to \gamma\eta_c$ ($\eta_c \to n\bar{n}$). None of these potential background sources exhibits peaking in the distribution of the angle between the n and $\bar{n}$.

B. Efficiency determination

We use specially chosen event samples from data to determine the efficiencies for each requirement in the $J/\psi \to n\bar{n}$ selection. The overall efficiency is then computed bin-by-bin in $\cos\theta$ as the product of these components and is applied as a correction in obtaining the angular distribution and branching fraction.

We select $J/\psi \to p\bar{n}\pi^-$ events to study the efficiency of the $\bar{n}$ selection. Events with exactly two good charged tracks identified as p and π^- are selected. Information from the TOF detector and dE/dx information from the MDC are combined to do the particle identification. The p and π^- are required to have a missing mass within 30 MeV of the nominal $\bar{n}$ mass. The missing momentum of the p and π^- is required to be in the range 1.1–1.2 GeV/c to ensure a sample that is as similar as possible to the $\bar{n}$ in $J/\psi \to n\bar{n}$ (momentum 1.232 GeV/c). The number of events passing the above selection gives $N^{\rm exp}$, the expected $\bar{n}$ yield. The number of $\bar{n}$ candidates selected from these events (criteria defined in Sec. VI A) that match the missing momenta of the accompanying p and π^- within 10° gives the observed yield $N^{\rm obs}$. The efficiency for $\bar{n}$ selection is $\epsilon_{\bar{n}}^{\rm data} = N^{\rm obs}/N^{\rm exp}$.

To validate this procedure and ensure consistency between the $\bar{n}$ in $J/\psi \to p\bar{n}\pi^-$ and that in the signal process $J/\psi \to n\bar{n}$, we select higher-purity $\bar{n}$ candidates in $J/\psi \to n\bar{n}$ ($J/\psi \to p\bar{n}\pi^-$) with a stringent cut of 177° on the angle between the n and $\bar{n}$. (For $J/\psi \to p\bar{n}\pi^-$ the cut is on the angle between the $\bar{n}$ and the missing momentum of the p and π^-.) Comparisons of the selection variables (energy deposit in EMC, number of EMC hits in a 50° cone about the $\bar{n}$ shower, and the shower second moment) for these two $\bar{n}$ samples are shown in Fig. 8. Each distribution is plotted after the cuts on the other variables have been imposed. There is good agreement, verifying that the $\bar{n}$ in $J/\psi \to p(\bar{n})\pi^-$ is a good match to the $\bar{n}$ in the signal process $J/\psi \to n\bar{n}$, and that this process provides a reliable efficiency correction.

We apply the same technique to calculate the efficiency for selecting the neutron ($\epsilon_n^{\rm data}$), in this case using a sample of $J/\psi \to \bar{p}(n)\pi^+$ selected from data. A comparison of the distribution of the EMC energy for neutrons from $J/\psi \to \bar{p}(n)\pi^+$ with that from $J/\psi \to n\bar{n}$ is shown in Fig. 9. In this case the momentum difference between the two n samples results in a greater difference in the EMC energy than was observed in the $\bar{n}$ case. This disagreement is a source of systematic error, which we try to minimize by the use of the very loose energy cut on the n shower.

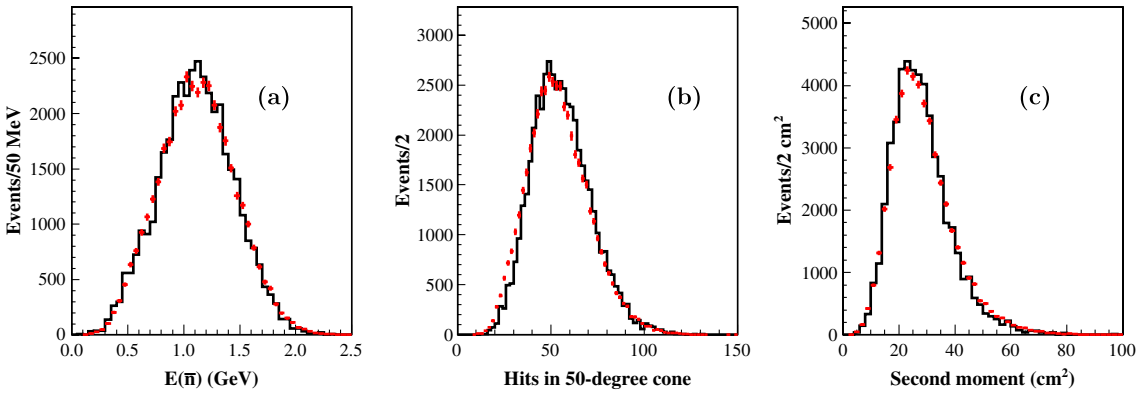

FIG. 8 (color online). Comparisons of distributions of selection variables for $\bar{n}$ from $J/\psi \to n\bar{n}$ (solid line) with those from $J/\psi \to p\bar{n}\pi^-$ (points): (a) deposited energy in the EMC, (b) the number of EMC hits in the 50° cone around the $\bar{n}$ shower, and (c) the second moment of the EMC energy deposit.

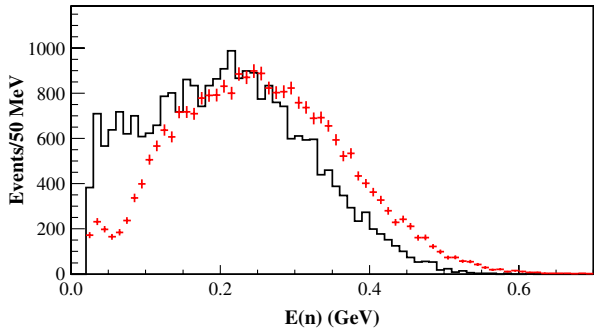

FIG. 9 (color online). Comparison of the distribution of the deposited energy in the EMC for n showers from $J/\psi \to n\bar{n}$ (points) with that from $J/\psi \to \bar{p}n\pi^+$ (solid line).

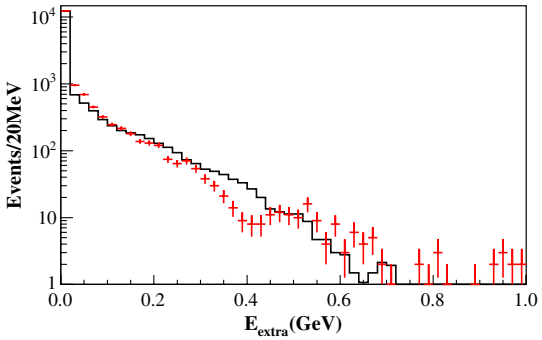

FIG. 10 (color online). Comparison of the distribution of $E_{\rm extra}$ in $J/\psi \to n\bar{n}$ (points) with that from $J/\psi \to p\bar{p}$ (solid line).

For the $E_{\rm extra}$ cut, we use $J/\psi \to p\bar{p}$ to obtain the efficiency ($\epsilon^{\rm data}_{E_{\rm extra}}$). The requirements are identical to those described in Sec. VA. Our selection of $J/\psi \to p\bar{p}$ does not depend on information from the calorimeter, so the behavior of $p\bar{p}$ in the EMC can be used to verify the efficiency of the $E_{\rm extra}$ cut for $J/\psi \to n\bar{n}$. Figure 10 shows the comparison of the $E_{\rm extra}$ distributions for $J/\psi \to p\bar{p}$ and $J/\psi \to n\bar{n}$. We require the angle between the n and $\bar{n}$ to be greater than 177° to suppress background for this comparison. We find that the proportion of $E_{\rm extra} = 0$ events in $J/\psi \to p\bar{p}$ and $J/\psi \to n\bar{n}$ agree well. The ratio of $J/\psi \to p\bar{p}$ events with or without the requirement $E_{\rm extra} = 0$ is calculated as the efficiency of the $E_{\rm extra}$ cut.

Finally, we determine the overall efficiency from the product of the three component efficiencies described above:

$$\epsilon = \epsilon^{\rm data}_{\bar{n}} \epsilon^{\rm data}_{n} \epsilon^{\rm data}_{E_{\rm extra}}.$$

To facilitiate measurement of the angular distribution as well as the yield, the product efficiency is determined in 16 bins in cosθ (cosine of the $\bar{n}$ polar angle) from -0.8 to 0.8. Figure 11 shows the efficiency for each cut and the product as a function of cosθ. The loss of $\bar{n}$ efficiency near cos$\theta = \pm 0.8$ is caused by the requirement on the number of EMC hits in a 50° cone around the shower. To smooth the bin-to-bin statistical fluctuations in the efficiency correction, we fit with a fifth-order polynomial [Fig. 11(d)].

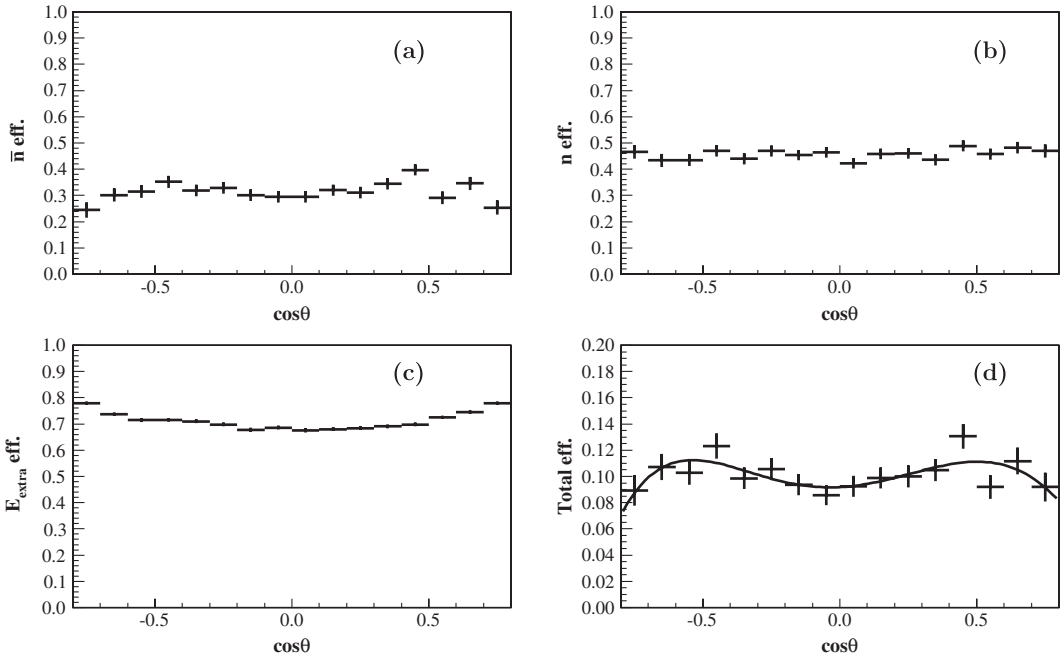

FIG. 11. Component selection efficiencies for $J/\psi \to n\bar{n}$ as a function of cosθ: (a) $\bar{n}$ selection, (b) n selection, and (c) $E_{\rm extra}$ cut; (d) overall product efficiency as computed (points) and smoothed by fitting to a fifth-order polynomial (line).

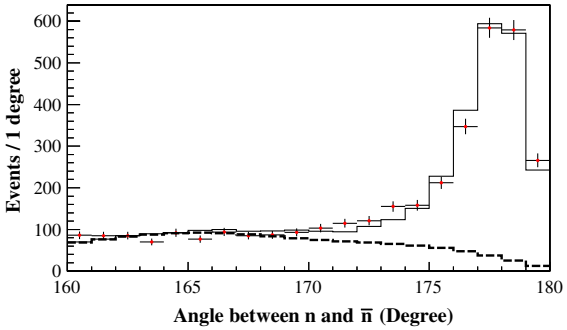

FIG. 12 (color online). Fit to the angle between the n and $\bar{n}$ for $\cos\theta$ in $[-0.3, -0.2]$.

C. Angular distribution and branching fraction

The number of $J/\psi \to n\bar{n}$ events in each $\cos\theta$ bin is obtained by fitting the distribution of the angle between the n and $\bar{n}$. The signal shape is determined with the $J/\psi \to p\bar{p}$ sample. Because of the 1.0-T magnetic field in the BESIII detector, the angular distribution in $J/\psi \to p\bar{p}$ must be corrected before being applied to $J/\psi \to n\bar{n}$. The signal shape (Ψ) for fitting the distribution of the angle between n and $\bar{n}$ can be expressed in terms of $d\theta_p$ ($d\theta_{\bar{p}}$) and $d\phi_p$ ($d\phi_{\bar{p}}$), the polar and azimuthal angles between the shower position and the extrapolated EMC position of p ($\bar{p}$), as follows:

$$\Psi = \sqrt{(1-\cos^2\theta_p)d\phi^2_{p\bar{p}} + d\theta^2_{p\bar{p}}},$$

where θ_p is the polar angle of the proton track, $d\theta_{p\bar{p}} = d\theta_p + d\theta_{\bar{p}}$ and $d\phi_{p\bar{p}} = d\phi_p + d\phi_{\bar{p}}$. The background shape is fixed to the shape of the inclusive background, while signal and background normalizations are allowed to float in each $\cos\theta$ bin. A sample fit for one $\cos\theta$ bin is shown in Fig. 12.

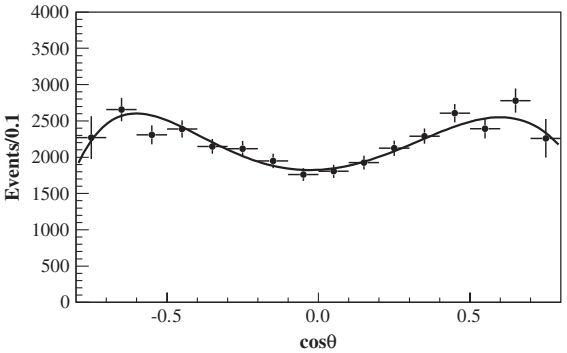

FIG. 13. The points represent the measured distribution of $\cos\theta$ for the $\bar{n}$ in $J/\psi \to n\bar{n}$ candidate events, with error bars that are the quadratic sums of the statistical and efficiency uncertainties. The line represents the fit of the distribution to the functional form given in the text, and is used to determine the normalization and the angular-distribution parameter α.

After obtaining the bin-by-bin signal yields, we fit the resulting $\cos\theta$ distribution with the function $A(1 + \alpha\cos^2\theta)\epsilon(\cos\theta)$, where A gives the overall normalization and $\epsilon(\cos\theta)$ is the corrected efficiency. The resulting angular distribution and fit are shown in Fig. 13. The χ^2 for the fit is 13 for 14 degrees of freedom, and the value determined for the angular-distribution parameter is $\alpha = 0.50 \pm 0.04$ (statistical error only).

The raw number of $J/\psi \to n\bar{n}$ events in the range $\cos\theta = [-0.8, 0.8]$ is $N(-0.8, 0.8) = 35891 \pm 211$. The efficiency-corrected yield obtained from the $\cos\theta$ fit is $N_{\rm cor}(-0.8, 0.8) = 354195 \pm 2078$. The fitted value of α is used to determine the total number of $J/\psi \to n\bar{n}$ events in the full angular range of $\cos\theta = [-1.0, 1.0]$ as follows:

$$N_{\rm cor}(-1.0, 1.0) = N_{\rm cor}(-0.8, 0.8) \times \frac{\int_{-1.0}^{1.0}(1 + \alpha\cos^2\theta)d\theta}{\int_{-0.8}^{0.8}(1 + \alpha\cos^2\theta)d\theta}$$
$$= 466590 \pm 2737.$$

Combining this total yield with the number of J/ψ events in our sample, we find the branching fraction to be

$$\mathcal{B}(J/\psi \to n\bar{n}) = (2.07 \pm 0.01) \times 10^{-3},$$

where the error is only statistical.

D. Systematic errors and results

The different $\bar{n}(n)$ momentum distributions in $J/\psi \to p\bar{n}\pi^-$ (c.c.) and $J/\psi \to n\bar{n}$ may introduce systematic uncertainties in the $\bar{n}(n)$ efficiency determination. We change the missing-momentum range from (1.1–1.2) GeV/c to (1.0–1.1) GeV/c when selecting the $\bar{n}(n)$ sample from $J/\psi \to p\bar{n}\pi^-$ (c.c.) and take the resulting differences in α and the branching fraction as systematic errors. This estimation is cross-checked with a lower-statistics sample obtained from a separate BESIII data sample collected at the $\psi(3686)$ resonance. High-momentum $\bar{n}(n)$ candidates are selected from the decay $\psi(3686) \to \pi^+\pi^- J/\psi$, $J/\psi \to p\bar{n}\pi^-$ (c.c.). The average $\bar{n}(n)$ efficiencies obtained with this sample are consistent with those from $J/\psi \to p\bar{n}\pi^-$ (c.c.) within statistical errors.

A second source of systematic error in the $\bar{n}$ (n) efficiency is the effect of the requirement that the shower be within 10° of the expected direction. We estimate the systematic errors due to this requirement by removing it and determining the changes in the results. We sum these two systematic error in quadrature to obtain the total systematic errors due to the selection of $\bar{n}$ (n). For the α determination, the $\bar{n}$ and n errors are 0.04 and 0.09, respectively, and for the branching fraction they are 5×10^{-5} and 1.2×10^{-4}. For the branching fraction the n efficiency is the largest source of uncertainty in our measurement.

As we did for $J/\psi \to p\bar{p}$, we use a toy MC method to estimate systematic errors due to the statistical uncertainties in the efficiency. For α, this systematic error is 0.17,

the largest contributor to the overall uncertainty of the measurement. For the branching fraction this error it is 7.1×10^{-5} and is the second-largest contributor.

We change the background shape for each exclusive MC background channel and repeat the fit of the angle between n and $\bar{n}$. The largest variation observed for any case considered is assigned as the systematic error.

Our signal shape in fitting the $n - \bar{n}$ angle was obtained from $J/\psi \to p\bar{p}$. The correction of the $p - \bar{p}$ angular distribution into one appropriate for $n - \bar{n}$ in $J/\psi \to n\bar{n}$ is a source of systematic uncertainty. To assess this we used a sideband subtraction instead of the fit to the angular distribution. We normalize the yield of MC background in the signal region (170°–180°) by the numbers of events in the sideband range (160°–170°) for data and MC background. Then we take the background-subtracted number of events in the signal region (170°–180°) as the yield in each $\cos\theta$ bin. The differences between this alternative method and the standard method are assigned as systematic errors.

The angular resolution can introduce systematic uncertainty both through the binning and through the $|\cos\theta| < 0.8$ cut. We use the $J/\psi \to p\bar{p}$ sample to evaluate the $\cos\theta$ resolution for $J/\psi \to n\bar{n}$. In the data $d\cos\theta = \cos\theta_{\bar{p}\text{ext}} - \cos\theta_{\bar{p}\text{emc}}$ is calculated as the equivalent of the resolution in $\cos\theta$ for $\bar{n}$, where $\cos\theta_{\bar{p}\text{ext}}$ represents the extrapolated position of the $\bar{p}$ at the EMC and $\cos\theta_{\bar{p}\text{emc}}$ is the reconstructed position in the EMC. Here we assume that the position reconstruction of $\bar{n}$ in the EMC is similar to that for $\bar{p}$, because both are dominated by hadronic interactions. To estimate the systematic error, we smear the $\cos\theta$ of $\bar{n}$ with the distribution of $d\cos\theta$ and redo the fit in each bin, and the fit to the angular distribution. The resulting changes are taken as the systematic errors.

For the all-neutral $n\bar{n}$ final state the trigger efficiency is another potential source of uncertainty. We correct the efficiency curve with the MC-determined trigger efficiency and redo the fit. The resulting changes in the branching fraction and α are taken as systematic uncertainties due to trigger efficiency.

To consider the systematic error from interference between the J/ψ peak and the continuum, we write the total cross section $\sigma_{n\bar{n}}$ as

$$\sigma_{n\bar{n}} = |\sqrt{\sigma^{\text{cont.}}_{n\bar{n}}} + \frac{\sqrt{12\pi\Gamma_{ee}\Gamma_{\text{tot}}}}{s - m^2 + im\Gamma_{\text{tot}}}(E_n - e^{i\phi}S)|^2,$$

where E_n and S are the EM and strong amplitudes for $J/\psi \to n\bar{n}$ and ϕ is the phase angle between them. $\sigma^{\text{cont.}}_{n\bar{n}}$ is the $n\bar{n}$ cross section contributed by continuum under the J/ψ peak. These values are taken from Sec. VII and, as discussed there, the EM amplitude E_n should be opposite to E_p. The cross section $\sigma(e^+e^- \to n\bar{n})$ close to J/ψ is assumed to lie between $\sigma(e^+e^- \to p\bar{p})$ and $\sigma(e^+e^- \to p\bar{p}) \cdot (\mu_n/\mu_p)^2$, so the E_n, which is in proportion to $\sqrt{\sigma^{\text{cont.}}_{n\bar{n}}}$, ranges from E_p to $E_p(\mu_n/\mu_p)$, where μ_n and μ_p are the magnetic moments of the neutron and proton. To estimate the uncertainty from the continuum, we take the larger one, $\sigma^{\text{cont.}}_{n\bar{n}} \sim \sigma^{\text{cont.}}_{p\bar{p}}$, therefore also $E_n \sim E_p$. The difference with and without $\sigma^{\text{cont.}}_{n\bar{n}}$ is assigned as systematic error.

Finally, we change α by $\pm 1\sigma$ (including the systematic error) and reevaluate the branching fraction to estimate the systematic error in the branching-fraction measurement.

Table III summarizes the systematic uncertainties and their sum in quadrature. The final results for our $J/\psi \to n\bar{n}$ measurements are as follows:

$$\alpha = 0.50 \pm 0.04 \pm 0.21, \quad \text{and}$$
$$\mathcal{B}(J/\psi \to n\bar{n}) = (2.07 \pm 0.01 \pm 0.17) \times 10^{-3}.$$

The branching-fraction measurement is consistent with the previous world average [6] and improves the overall precision by about a factor of 2.3.

TABLE III. Systematic errors for $J/\psi \to n\bar{n}$.

Sources	Effect on α	Effect on $\mathcal{B}$ (10^{-3})
$\bar{n}$ selection	0.04	0.05
n selection	0.09	0.12
Efficiency correction statistics	0.17	0.07
Background	0.03	0.03
Signal shape	0.02	0.06
$\cos\theta$ resolution	0.05	0.01
Trigger	0.03	0.01
α value	...	0.01
Number of J/ψ	...	0.03
Continuum	...	0.01
Total	0.21	0.17

VII. SUMMARY

We have used the world's largest sample of J/ψ decays to make new measurements of the branching fractions and production-angle distributions for $J/\psi \to p\bar{p}$ and $J/\psi \to n\bar{n}$, obtaining the branching fractions $\mathcal{B}(J/\psi \to p\bar{p}) = (2.112 \pm 0.004 \pm 0.031) \times 10^{-3}$ and $\mathcal{B}(J/\psi \to n\bar{n}) = (2.07 \pm 0.01 \pm 0.17) \times 10^{-3}$. These results represent significant improvements over previous measurements. The angular distributions for both decays are well described by the functional form $1 + \alpha\cos^2\theta$, with measured values of $\alpha = 0.595 \pm 0.012 \pm 0.015$ for $J/\psi \to p\bar{p}$, and $\alpha = 0.50 \pm 0.04 \pm 0.21$ for $J/\psi \to n\bar{n}$.

The $p\bar{p}$ angular distribution can be decomposed as $|C_p^M|^2(1 + \cos^2\theta) + (2M_p/M_{J/\psi})^2|C_p^E|^2\sin^2\theta$, where C_p^M and C_p^E are the total helicity ± 1 and 0 decay amplitudes. In terms of the angular parameter α, the ratio of amplitudes is $|C_p^E/C_p^M| = M_{J/\psi}/(2M_p)\sqrt{(1-\alpha)/(1+\alpha)}$. With our measured values for α, we find $|C_p^E/C_p^M| = 0.832 \pm 0.015 \pm 0.019$ and $|C_n^E/C_n^M| = 0.95 \pm 0.05 \pm 0.27$,

respectively. These measurements permit discrimination among the different proposed models [24–30].

The relative phase between the strong and EM amplitudes can be obtained by comparing $\mathcal{B}(J/\psi \to p\bar{p})$ and $\mathcal{B}(J/\psi \to n\bar{n})$. The J/ψ EM decay amplitudes are related to the corresponding continuum cross sections close to the J/ψ as follows: $E_N^2(J/\psi \to \gamma^* \to N\bar{N}) = \mathcal{B}(J/\psi \to \mu\mu) \cdot \sigma(e^+e^- \to N\bar{N})/\sigma(e^+e^- \to \mu\mu)$. Present data [31] suggest that $\sigma(e^+e^- \to p\bar{p}) \sim (9 \pm 3)$ pb, if fitted with a smooth W^{-10} as expected at high enough center-of-mass energies W. For $\sigma(e^+e^- \to n\bar{n})$ the only available data [32,33] are close to threshold. In the following it is assumed that the neutron timelike dominant magnetic form factor is negative at these center-of-mass energies, like the magnetic moment, as predicted dispersion relations [34]. The cross section $\sigma(e^+e^- \to n\bar{n})$ close to J/ψ is assumed to lie between $\sigma(e^+e^- \to p\bar{p})$, as is seen in the present data close to threshold, and $\sigma(e^+e^- \to p\bar{p}) \cdot (\mu_n/\mu_p)^2$, as in the spacelike region [35]. Taking into account these hypotheses and their overall uncertainties, and neglecting the contribution of continuum amplitudes, the strong amplitude S is given by

$$\begin{aligned} S^2 &= [(\mathcal{B}(J/\psi \to p\bar{p}) - E_p^2)E_n \\ &\quad + (\mathcal{B}(J/\psi \to n\bar{n}) - E_n^2)E_p]/(E_n + E_p) \\ &= (2.038 \pm 0.094) \cdot 10^{-3}, \end{aligned}$$

and the phase ϕ between the strong and EM amplitudes is found to be

$$\begin{aligned} \phi &= \cos^{-1}[(\mathcal{B}(J/\psi \to p\bar{p}) - S^2 - E_p^2)/(2SE_p)] \\ &= (88.7 \pm 8.1)^\circ. \end{aligned}$$

The uncertainty in the phase is mostly due to the $\mathcal{B}(J/\psi \to n\bar{n})$ systematic error. This determination confirms the orthogonality of the strong and EM amplitudes within the precision of our measurement.

ACKNOWLEDGMENTS

The BESIII collaboration thanks the staff of BEPCII and the computing center for their hard efforts. This work is supported in part by the Ministry of Science and Technology of China under Contract No. 2009CB825200; Joint Funds of the National Natural Science Foundation of China under Contracts Nos. 11079008, 11179007; National Natural Science Foundation of China (NSFC) under Contracts Nos. 10625524, 10821063, 10825524, 10835001, 10935007, 11125525; the Chinese Academy of Sciences (CAS) Large-Scale Scientific Facility Program; CAS under Contracts Nos. KJCX2-YW-N29, KJCX2-YW-N45; 100 Talents Program of CAS; Istituto Nazionale di Fisica Nucleare, Italy; U. S. Department of Energy under Contracts Nos. DE-FG02-04ER41291, DE-FG02-91ER40682, DE-FG02-94ER40823, DE-FG02-05ER41374; U.S. National Science Foundation; University of Groningen (RuG) and the Helmholtzzentrum fuer Schwerionenforschung GmbH (GSI), Darmstadt; WCU Program of National Research Foundation of Korea under Contract No. R32-2008-000-10155-0

[1] R. Baldini, C. Bini, and E. Luppi, Phys. Lett. B **404**, 362 (1997).
[2] C. Z. Yuan, P. Wang, and X. H. Mo, Phys. Lett. B **567**, 73 (2003).
[3] P. Wang, C. Z. Yuan, and X. H. Mo, Phys. Rev. D **69**, 057502 (2004).
[4] V. L. Chernyak and I. R. Zhitnitsky, Nucl. Phys. **B246**, 52 (1984).
[5] C. Carimalo, Int. J. Mod. Phys. A **2**, 249 (1987).
[6] K. Nakamura *et al.* (Particle Data Group), J. Phys. G **37**, 075021 (2010).
[7] A. Antonelli *et al.* (FENICE Collaboration), Phys. Lett. B **334**, 431 (1994).
[8] M. Ablikim *et al.* (BESIII Collaboration), Nucl. Instrum. Methods Phys. Res., Sect. A **614**, 345 (2010).
[9] D. M. Asner *et al.*, *Physics at BESIII*, edited by K. T. Chao and Y. F. Wang [Int. J. Mod. Phys. A 24, S1 (2009)].
[10] M. Ablikim *et al.* (BESIII Collaboration), Phys. Rev. D **83**, 012003 (2011).
[11] S. Agostinelli *et al.* (GEANT4 Collaboration), Nucl. Instrum. Methods Phys. Res., Sect. A **506**, 250 (2003). Geant4 version: v09-03p0; Physics List simulation engine: BERT; Physics List engine packaging library: PACK 5.5.
[12] J. Allison *et al.*, IEEE Trans. Nucl. Sci. **53**, 270 (2006).
[13] R. G. Ping, Chinese Phys. C **32**, 8 (2008).
[14] D. J. Lange, Nucl. Instrum. Methods Phys. Res., Sect. A **462**, 152 (2001).
[15] Giovanni Balossini *et al.*, Nucl. Phys. **B758**, 227 (2006).
[16] S. Jadach, B. F. L. Ward, and Z. Was, Comput. Phys. Commun. **130**, 260 (2000); Phys. Rev. D **63**, 113009 (2001).
[17] T. Sjostrand, Comput. Phys. Commun. **82**, 74 (1994).
[18] I. Peruzzi *et al.*, Phys. Rev. D **17**, 2901 (1978).
[19] M. W. Eaton *et al.*, Phys. Rev. D **29**, 804 (1984).
[20] J. S. Brown, Ph.D. thesis, University of Washington, 1984.
[21] R. Brandelik *et al.*, Physica C (Amsterdam) **1**, 233 (1976).
[22] D. Pallin *et al.* (DM2 Collaboration), Nucl. Phys. **B292**, 653 (1987).
[23] J. Z. Bai *et al.* (BES Collaboration), Phys. Lett. B **591**, 42 (2004).
[24] M. B. Wise, M. Claudson, and S. L. Glashow, Phys. Rev. D **25**, 1345 (1982).

[25] V. L. Chernjak and J. R. Zhitnisky, Phys. Rep. **112**, 173 (1984).
[26] M. Gari and N. G. Stefanis, Phys. Lett. B **175**, 462 (1986).
[27] I. D. King and C. T. Sachraida, Nucl. Phys. **B279**, 785 (1987).
[28] C. Carimalo, Int. J. Mod. Phys. A **2**, 249 (1987).
[29] V. L. Chernjak, A. A. Oglobi, and J. R. Zhitnisky, Z. Phys. C **42**, 565 (1989).
[30] N. G. Stefanis and M. Bergmann, Phys. Rev. D **47**, R3685 (1993).
[31] B. Aubert *et al.* (*BABAR* Collaboration), Phys. Rev. D **73**, 012005 (2006).
[32] A. Antonelli *et al.* (FENICE Collaboration), Nucl. Phys. **B517**, 3 (1998).
[33] Alexander E. Obrazovsky, (on behalf of the SND collaboration) *Proceedings of the XIV International Conference on Hadron Spectroscopy* (Munich, Germany, 2011), pp. 13–17.
[34] R. Baldini, S. Dubnicka, P. Gauzzi, S. Pacetti, E. Pasqualucci, and Y. Srivastava, Eur. Phys. J. C **11**, 709 (1999).
[35] John Arrington, *Proceedings of QCD Bound States Workshop* (Argonne National Lab, Argonne, IL, 2009), pp. 15–19.